

# Simple Demonstrations of Pattern Formation

Stephen J. Van Hook and Michael F. Schatz

One of the most striking and beautiful behaviors in the world around us is the way systems in nature take their shape. This process of pattern formation occurs in a wide variety of systems, including sand, flames, lasers, fractures, river networks, chemical reactions, and growing organisms (morphogenesis). In many instances, the patterns share common features and similar shapes appear repeatedly (e.g., stripes, hexagons, squares, and spirals). The important role of instabilities in pattern formation can be demonstrated in visually appealing experiments for an introductory physics classroom. In addition, simple experiments on pattern formation can be used for low-cost undergraduate laboratory projects in the study of instabilities.

In this paper, we describe how pattern-forming behaviors can be easily demonstrated in two fluid experiments that played pivotal roles in the development of fundamental concepts in pattern formation. Experiments in fluids provide the best understood pattern-forming examples since the governing equations and control parameters of fluid systems are known, experimental conditions can be well defined and easily controlled, and the patterns can be readily visualized.

## General Features of Pattern Formation

Patterns often appear or change when the physical system crosses a threshold condition, similar to a phase change at a boiling or melting point. In typical experiments, there are one or more control parameters that permit the experimental conditions to be varied continuously. At well-defined (critical) values of the control parameters, patterns appear or change spontaneously due to an *instability*; the system is said to undergo a bifurcation or transition.

These transitions differ qualitatively from equilibrium phase transitions (e.g. the freezing of a liquid), however. Equilibrium phase transitions are governed by the minimization of a free energy; pattern forming bifurcations arise when a system is driven far from thermodynamic equilibrium to where no free energies are expected to exist. The control parameters characterize the strength of the nonequilibrium driving; in the experiments we discuss, the

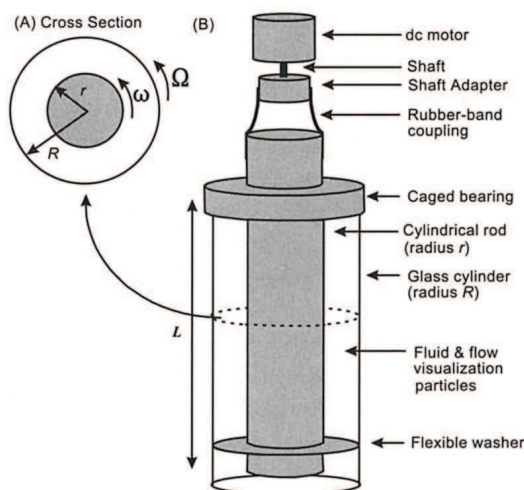


Fig. 1A. Taylor-Couette demonstration, horizontal cross section. Fluid is confined between inner cylinder of radius  $r$  and outer cylinder of radius  $R$ . Inner and outer cylinders may independently rotate with angular velocities  $\omega$  and  $\Omega$ , respectively. B. Schematic of Taylor-Couette demonstration apparatus.

parameters can also be interpreted as a measure of the competition between driving and dissipative mechanisms; the driving mechanism “wins” at the appearance (onset) of the bifurcation and a new pattern forms.

## Taylor-Couette Flow between Rotating Cylinders

In 1923, Geoffrey I. Taylor performed a comprehensive study of instability in rotating fluid flow that Sir Isaac Newton had described



**Stephen J. Van Hook** received his Ph.D. in physics from the University of Texas at Austin in 1996 and is currently studying pattern formation and surface-tension-driven instabilities as a post-doctoral researcher. He is particularly interested in physics education at all grade levels and increasing the interest in science by the general public. Center for Nonlinear Dynamics and Department of Physics, University of Texas at Austin, Austin, TX 78712; svanhook@chaos.ph.utexas.edu.



schematically in the *Principia*.<sup>1</sup> The fluid was confined between two concentric cylinders that could be rotated independently (Fig. 1). Using dye injected into the flow, Taylor observed structureless azimuthal flow (Couette flow) for small rotation rates (Fig. 2A). However, as the rotation rate increased, Taylor observed the abrupt appearance of donut-shaped vortices (Taylor vortices) that encircled the inner cylinder (Fig. 2B). Taylor's theoretical analysis of

As the inner cylinder rotates, an annulus of fluid near the inner cylinder begins to rotate in the same direction, and at the same time tends to fly radially outward due to centrifugal forces. The centrifugal force per unit volume of fluid is  $\sim \rho r \omega^2$  with fluid density  $\rho$ , inner cylinder radius  $r$ , and angular velocity  $\omega$ . The viscosity of the fluid produces frictional forces that oppose the action of the centrifugal forces; this viscous friction per unit volume of fluid is

$\sim \rho \nu \omega / r$  with the kinematic viscosity  $\nu$  (with dimensions of length squared divided by time).<sup>4</sup> The strength of the centrifugal forces (the driving mechanism) relative to the friction (the dissipative mechanism) is, therefore,  $(\rho r \omega^2) \times (r / \rho \nu \omega) = \omega r^2 / \nu \equiv Re$ , the Reynolds number, which is the control parameter for Taylor-Couette flow.

In an experiment,  $Re$  is varied by varying  $\omega$ . For  $Re$  sufficiently small ( $\omega$  small), friction suppresses the centrifugal effects and purely azimuthal flow (Couette flow) results. For  $Re$  sufficiently large ( $\omega$  large), however, the centrifugal forces overcome the friction, fluid flows axially and radially as well as azimuthally, and Taylor vortices form. This qualitative change in behavior (bifurcation) occurs at a well-defined value of  $Re$  known as the critical value,  $Re_c$ . Note that this bifurcation arises at the same value of  $Re_c$  for a variety of different experimental conditions (different fluids, different rotation speeds, etc.).<sup>5</sup> As  $Re$  is increased further, the system undergoes a series of bifurcations to new states until the flow eventually becomes turbulent

(Fig. 2C). (A phase diagram of possible states can be found in Ref. 4.)

You can demonstrate Taylor-Couette flow (with  $\Omega = 0$ ) by constructing a simple apparatus from the following components (see Fig. 1):

- a 100-ml graduated cylinder
- a cylindrical rod ( $\sim 1 \frac{1}{4}$  cm diameter, 20 cm long)
- a flexible washer (e.g., a garden-hose washer)
- a  $\frac{1}{2}$ -in ID (R8VV) caged bearing
- a thick ( $\sim \frac{1}{2}$  cm wide) rubber band
- a small dc motor (e.g., Radio Shack No. 273-256)

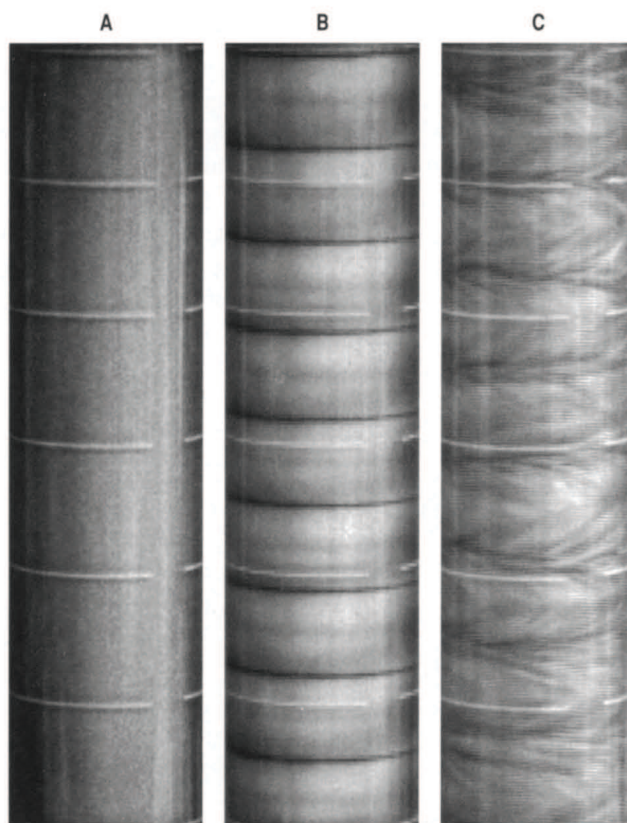


**Fig. 2. Sequence of flows from Couette flow to turbulence using aluminum powder in water/glycerol mixture. White horizontal lines are 10-ml marks (1.9 cm apart) on graduated cylinder. A. Couette flow ( $Re \sim 25$ ); B. Taylor vortices ( $Re \sim 300$ , 9 vortices); C. turbulent Taylor vortices ( $Re \sim 4000$ , 8 vortices).**

the flow yielded the first predictions for the onset of a pattern in a physical system that is in quantitative accord with experimental observations. For this reason, this experiment is known as Taylor-Couette flow.<sup>2</sup> (In 1890, M. Couette used this flow to determine fluid viscosities; this technique is still in widespread use.) Later experiments in Taylor-Couette flow yielded the first convincing evidence for the existence of chaos (i.e., deterministic unpredictable behavior) in nature.<sup>3</sup>

To understand the physical cause of the Taylor vortices, consider the special case where the outer cylinder is at rest ( $\Omega = 0$  in Fig. 1A).



**Michael Schatz** is an assistant professor in the school of physics at the Georgia Institute of Technology. He has a B.S. in physics from the University of Notre Dame and a Ph.D. in physics from the University of Texas at Austin. His research area is nonlinear dynamics, with emphasis on experimental studies of pattern formation and of complex behavior in spatially extended systems. His current teaching interests focus on implementing and assessing active learning techniques for large introductory physics lectures. School of Physics, Georgia Institute of Technology, Atlanta, GA 30332  
michael.schatz@physics.gatech.edu



- potentiometer (e.g., 50  $\Omega$ )
- a battery or dc power supply
- electrical tape

The inner cylinder (rod) must be held firmly at the center of the outer cylinder (graduated cylinder) and yet be allowed to rotate freely. Restrict the lateral movement of the rod by installing the caged bearing at the top of the graduated cylinder and a flexible washer near the bottom. The flexible washer should press against the outer cylinder and have an inner diameter slightly larger than the diameter of the rod so that the rod can rotate freely without significant radial motion. The caged bearing should fit tightly on the rod so that the rod is suspended above the bottom of the graduated cylinder. The bearing is then secured to the top of the graduated cylinder with electrical tape. Couple the rod to the motor shaft by short strips cut from a thick rubber band; the strips provide a flexible connection so that precise alignment between the motor and the rod is unnecessary. If the radius of the motor shaft is much smaller than  $r$ , you can wrap electrical tape symmetrically around the motor shaft to increase its diameter to a size that enables connection of the rubber band strips.

Fill the graduated cylinder with liquid before inserting the rod. Vegetable oil has a high viscosity suitable for demonstrating the transition to Taylor vortices, whereas

Bronze or aluminum powder flakes suspended in the fluid will reveal the flow pattern. You can purchase bronze powder directly from a hardware or arts supply store.<sup>7</sup> Aluminum powder appropriate for visualization is harder to purchase directly (the powder must be in the form of flakes rather than grains); however, we found a hobby paint pigment that was well suited for revealing the flow patterns.<sup>8</sup> To prevent clumping, add a small amount of liquid soap to the powder before adding to aqueous liquids (this is not necessary with oil). For optimum visualization, perform the demonstration as soon as possible after mixing, since the powder will eventually settle to the bottom of the graduated cylinder.

## Bénard Convection

Diverse patterns can also arise in thin pools of liquid heated uniformly from below (Fig. 3). In his physics Ph.D. dissertation work at the turn of this century, Henri Bénard conducted the first laboratory experiment in pattern formation. Bénard found that, for sufficiently large heating, convection would spontaneously arise in an initially quiescent fluid and organize into a set of polygonal cells. More than a half a century elapsed before J.R.A. Pearson developed a theory that explained how surface tension forces caused the patterns observed by Bénard.<sup>9</sup> Earlier, Lord Rayleigh proposed that the fluid motion in Bénard's experiment was driven by buoyancy forces,<sup>4,9</sup> but Rayleigh's computations of the heating necessary for pattern formation did not agree with Bénard's observations. Nevertheless, buoyancy also can cause patterns and is responsible for pattern formation in many modern studies of thermal convection.

Buoyancy and surface tension drive convection in significantly different ways. Buoyancy can cause flow because warm fluid near the bottom of the liquid pool becomes less dense as it expands; the warm liquid then tends to rise and the cooler, more dense liquid at the top of the pool tends to fall (Fig. 3A). This process continues indefinitely since fluid is continually warmed by the heated surface at the bottom of the pool; therefore, convective flow results if the heating is sufficiently large. The buoyancy force per unit volume of fluid is  $\sim \rho \alpha g \Delta T$  with the fluid density  $\rho$ , the temperature coefficient of volume expansion  $\alpha$ , the gravitational acceleration  $g$ , and the temperature difference between the bottom and the top of the pool  $\Delta T$ . Surface tension can cause flow whenever the temperature varies along the top of the pool. Since surface tension generally decreases with temperature, warm spots at the top will have lower surface tension than cool spots at the top; the resulting difference in surface tension will cause flow from the warm spots to the cool spots (Fig. 3B). Since the fluid pulled from the warm regions at the top is replaced by fluid from below that is heated, the difference in surface tension and, hence, the flow, is sustained if the heating from below is sufficiently large. The surface tension force per

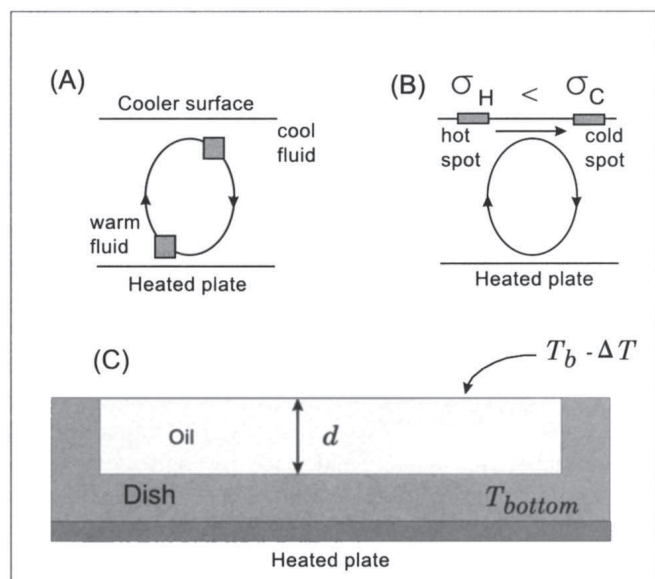


Fig. 3A. buoyancy driving mechanism for convection; B. surface-tension driving mechanism for convection; C. schematic of a simple Bénard convection cell.

water's low viscosity permits observation of turbulent flow for even small rotation rates. Alternatively, you can mix water with differing amounts of glycerol (also referred to as glycerin) to select the viscosity over a wide range. Glycerol can be obtained from a local pharmacy or science supply catalog;<sup>6</sup> a 30% water/70% glycerol mixture by weight is suitable for initial experiments.

unit volume of fluid is  $\sigma_T \Delta T / d^2$  with the pool depth  $d$ , surface tension  $\sigma$ , and  $\sigma_T \equiv -d\sigma/dT$ . The ratio of the surface tension forces to the buoyancy  $\sigma_T / \rho g \alpha d^2$  determines which effect is paramount. In an experiment this is most easily varied by changing  $d$ . Thus, for thin convecting layers ( $< \sim 1$  mm deep) surface tension dominates whereas buoyancy is more important for thicker layers.

Friction and thermal diffusion oppose both driving mechanisms; the balance between driving and dissipation yields a control parameter for each of the buoyancy and the surface-tension cases. As in the Couette-Taylor system, frictional forces arise in convection from the viscosity of the fluid. In addition, hot spots are smoothed out as heat is carried away by molecular motion (thermal diffusion), reducing the temperature gradients within the fluid that drive convection. Both effects combine to yield a dissipative force per unit volume  $\sim \rho \nu \kappa / d^3$ , where  $\kappa$  is the thermal diffusivity of the fluid. The strength of the driving force relative to the dissipative forces is  $(\rho \alpha g \Delta T) \times (d^3 / \rho \nu \kappa) = \alpha g \Delta T d^3 / \nu \kappa \equiv \text{Ra}$ , the Rayleigh number, which is the control parameter for the buoyancy-dominated case,  $(\sigma_T \Delta T / d^2) \times (d^3 / \rho \nu \kappa) = \sigma_T \Delta T d / \rho \nu \kappa \equiv \text{Ma}$ , the Marangoni number, which is the control parameter for the surface-tension dominated case.

The bifurcations leading to the formation of patterns in convection require a finite value of control parameter. In an experiment, Ra and Ma can be continuously changed by varying  $\Delta T$ ; for Ra and Ma that exceed the critical values  $\text{Ra}_c$  and  $\text{Ma}_c$ , the buoyancy and surface tension forces overcome the dissipative forces, fluid begins to flow, and patterns form. When surface tension is dominant, the initial patterns are cellular polygons with primarily a hexagonal symmetry (see cover), as first observed by Bénard. When buoyancy is dominant, the initial state can be either hexagons or stripes (“rolls”), depending on the upper boundary. With a free upper surface, hexagonal cells are the initial pattern. In all cases the patterns arise at the same value of  $\text{Ra}_c$  or  $\text{Ma}_c$  for a variety of different experimental conditions (e.g., different fluids, different  $\Delta T$ ).

You can demonstrate Bénard convection with an apparatus consisting of an open dish and a heating element (see Fig. 3C). A variety of configurations are possible, including:

*A simple home experiment.* A skillet with an approximately 1-mm layer of vegetable oil can be heated gently on a stove to induce convection.<sup>9</sup> The patterns can be visualized by sprinkling a powdered spice (e.g., cinnamon) on the surface of the fluid.

*Quick classroom demonstration.* Use a glass Petri dish and a hot plate to heat a layer of silicone oil. Mix aluminum or bronze powder (described earlier for Couette-Taylor experiments) into the oil; the detailed structure of the flow pattern shows more clearly than in the kitchen-spice visualization. (Do *not* use metal powder in dishes that will later be used for cooking.) Surface tension in most liquids other than silicone oil

will cause the powder to form a surface film, which ruins the visualization. Silicone oils are commercially available in a large range of viscosities;<sup>10</sup> a viscosity of  $0.5 \text{ cm}^2/\text{s}$  will keep the powder in suspension long enough to perform the demonstration, without requiring unreasonably large temperatures. The more uniform the temperature of the bottom plate, the better the appearance of the cells. For best results, we recommend placing a metal plate (about 1 cm thick) on top of the hot plate; the silicone oil rests on this metal plate and is contained by a lateral sidewall, which can be something as simple as an O-ring held to the metal plate with glue or grease.

## Exploring Pattern Formation

The demonstrations for Taylor-Couette flow and Bénard convection are versatile enough to examine qualitatively a wide range of patterning behaviors. For example:

*What is a typical size (length scale) of the pattern?*

Compare this with the length scale set by the boundaries of the experiment (i.e., the layer depth  $d$  in Bénard convection and the radii  $r$  and  $R$  in Taylor-Couette flow.) Change the boundary length scale and observe how the pattern length scale changes.

*How does the first appearance of a pattern depend on the experimental conditions?* Try changing the length scale or the liquid viscosity. Does the pattern arise with more or less driving (higher or lower  $\omega$ ,  $\Delta T$ )?

*Are the patterns unique for a fixed experimental configuration?* Are the number and shape of the cells the same at the first appearance of the pattern? Does the final pattern appearance depend on the rate at which the control parameter ( $\omega$ ,  $\Delta T$ ) is varied in time? After the pattern appears, does it keep the same form or does the pattern change in time?

*How do the patterns change as the control parameter is changed?* How many different patterns can be distinguished? How do they differ from the patterns that appear at onset? Try changing the experimental setup (length scale, fluid viscosity) and see if there are changes to the sequence of patterns that appear with increasing control parameter.

Video imaging provides a valuable tool to examine the spatial and temporal behavior of patterns. Patterns recorded with a home video camera can help reveal mechanisms by which the patterns evolve when played back later (at differing speeds). The multimedia capabilities of modern computers provide an inexpensive means for capturing pattern images; the video signal from a home video camera can be digitized using an inexpensive ( $< \$100$ ) frame grabber. The digitized images can then be analyzed quantitatively to obtain the pattern length scales and morphology. Moreover, “time-lapse” images can be recorded and sequenced to yield a movie that illustrates the longtime behavior of the pattern.

These demonstration experiments combined with video imaging would be suitable for an undergraduate research project, provided an accurate determination of the experimental conditions were made throughout the run. Some experimental conditions (e.g., the physical properties of the liquid) can be obtained from a suitable reference;<sup>11,12</sup> other conditions (e.g.,  $\omega$  and  $\Delta T$ ) need to be continually measured as they are changed.

## Conclusions

Pattern formation is a rapidly growing area of research and one ideally suited for undergraduate exploration in demonstrations such as described here. A reading of the pattern-formation literature should provide the reader with ideas for other demonstration experiments.<sup>13,14</sup>

## Acknowledgments

The authors acknowledge the support of NASA Grant NAG3-1382 and author Van Hook acknowledges the support of the NASA Graduate Student Researcher's Project.

## References

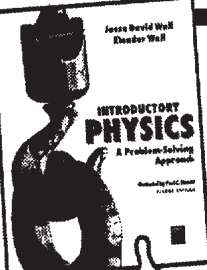
1. R.J. Donnelly, *Phys. Today* **44**, 32 (1991).
2. For an extensive bibliography of papers on this subject, see R. Tagg, "A guide to literature related to the Taylor-Couette problem," in *Ordered and Turbulent Patterns in Taylor-Couette Flow*, edited by C.D. Andereck and F. Hayot, *Proceedings of a NATO Advanced Workshop* (Plenum, 1992).
3. J. Gleick, *Chaos* (Viking Press, New York, 1987).
4. D.J. Tritton, *Physical Fluid Dynamics*, 2nd ed. (Oxford University Press, New York, 1988).
5. The radius ratio  $r/R$  is assumed to be fixed; this condition is typically satisfied in experiments.
6. A one-liter bottle of glycerin costs \$29.10 in the 1996–1997 Fisher Science Education Catalog; (800) 955-1177.
7. Bronze powder is manufactured by the Leo Uhlfelder Co., Mt. Vernon, New York 10553.
8. The pigment was obtained from a 1/4-oz. bottle of Testors Flat Enamel Paint (color 1181-aluminum) by allowing the pigment to settle to the bottom of the bottle and pouring off the excess liquid. The pigment was then washed several times in a volatile solvent (we used acetone—nail-polish remover) and left to dry before use as flow visualization. If needed in large quantities, aluminum powder flakes can be purchased from Skylighter, P.O. Box 480, Round Hill, VA 22141; (540) 554-4543.
9. P.G. Drazin and W.H. Reid, *Hydrodynamic Stability* (Cambridge University Press, Cambridge, 1981).
10. Dow Corning 200 silicone oils (dimethylpolysiloxane) can be purchased in small amounts from the Sigma Chemical Company, P.O. Box 14508, St. Louis, MO 63178; (800) 325-3010. Viscosities from 5–60,000 cS ( $10^{-2}$  cm<sup>2</sup>/s) are available for \$13.85/100 grams.
11. *Physics Vade Mecum* (American Institute of Physics, New York, 1981).
12. *CRC Handbook of Chemistry and Physics* (CRC Press, Boca Raton, FL, 1985).
13. H.M. Jaeger, S.R. Nagel, and R.P. Behringer, *Phys. Today* **49**, 32 (1996).
14. T.M. Pritchett and J.K. Kim, *Announcer*, **25**, 51 (1995).

**Get hooked!**  
A one semester introduction  
emphasizing  
**Problem Solving**

**INTRODUCTORY  
PHYSICS**  
A Problem-Solving Approach  
Jesse David Wall  
Elender Wall

**Analog Press**  
225 Edna Street  
San Francisco, CA  
(415) 239-2338  
email: analog@bayweb.net

Now in 2nd Edition



Illustrated by  
**PAUL G. HEWITT**

**More illustrations  
Twice as many problems  
New chapter on E&M fields  
More history of measurement**

